DOI 10.1007/s11015-023-01561-w
Metallurgist, Vol. 67, Nos. 5-6, September, 2023 (Russian Original Nos. 5-6, May–June, 2023)

IMPACT TOUGHNESS AND MICROSTRUCTURE OF LOW-ALLOY STEEL WELD PRODUCED BY AUTOMATIC SUBMERGED ARC WELDING

M. M. Kantor,[1] K. G. Vorkachev,[2] P. P. Stepanov,[3] S. V. Zharkov,[4] L. I. Efron,[5] and V. A. Bozhenov[6]

UDC 620.186:621.791.051.6:539.551

The impact toughness, microstructure and break features of low-alloy steel weld samples produced by automatic submerged arc welding have been compared. It has been established that when a notch is applied along the weld axis, fracture occurs along large grains of grain-boundary ferrite 80–140 μm in size with an unfavorable cleavage planes orientation {001}. The combination of such grains with non-metallic inclusions 3–5 μm in size facilitates the transcrystalline cleavage initiation. The effect of austenite grain size, crystallographic texture, and intergranular fracture on the impact toughness value is shown. Continuous chains of grain-boundary ferrite at the front of the main crack line up along the notch-parallel boundaries of columnar grains of axial orientation, which increases the tendency to transcrystalline cleavage. At the same time, with the lateral orientation of the columnar grains of the former austenite, the front line of the main crack intersects only certain separate areas of the grain-boundary ferrite. Offset notch results in an increase in both impact toughness and plasticity of weld metal.

Keywords: large diameter pipes, low-alloy steel, weld, Charpy impact, microstructure, crystallographic texture.

Introduction

In the process of multi-arc double-sided submerged arc welding of a pipe billet, a complex cast microstructure is formed [1–3]. Along the axis of the weld, columnar grains of the former austenite of axial orientation are formed. Columnar austenite grains of lateral orientation grow from the edges of the welded metal in the direction of the maximum temperature gradient. The results of measuring the impact strength depend on the location of the notch in the welded joint [4, 5]. Reduced values of impact strength in the center of the cast zone of the weld are associated with the formation of columnar grains of axial orientation [6]. However, the mechanism of this embrittlement is still insufficiently studied.

The favorable microstructure of the cast zone of the welded joint consists mainly of acicular ferrite (AF) located inside the former austenite grains, and a certain amount of grain-boundary ferrite (GBF), which forms a three-dimensional grid along the boundaries of the former austenite grains [7–11]. The conditions for the formation of acicular ferrite are considered to be the existence of a large number of suitable non-metallic inclusions

[1] A. A. Baikov Institute of Metallurgy and Materials Science of Russian Academy of Sciences, Moscow, Russia; e-mail: MKantor@imet.ac.ru.

[2] A. A. Baikov Institute of Metallurgy and Materials Science of Russian Academy of Sciences, Moscow, Russia; e-mail: kgv@imet.ac.ru.

[3] Vyksa Metallurgical Plant, Vyksa, Nizhny Novgorod Region, Russia; e-mail: Stepanov_PP@vsw.ru.

[4] Vyksa Metallurgical Plant, Vyksa, Nizhny Novgorod Region, Russia; e-mail: Zharkov_SV@vsw.ru.

[5] Vyksa Metallurgical Plant, Vyksa, Nizhny Novgorod Region, Russia; e-mail: LEfron@omk.ru.

[6] A. A. Baikov Institute of Metallurgy and Materials Science of Russian Academy of Sciences, Moscow, Russia; e-mail: VBozhenov@imet.ac.ru.

Translated from Metallurg, Vol. 67, No. 6, pp. 5–15, June, 2023. Original article submitted May 3, 2023, revised article submitted May 10, 2023, original article accepted May 25, 2023.

in austenite and a sufficient cooling rate in the range of $\gamma \rightarrow \alpha$ transformation [1–3, 12]. During impact bending tests, cleavage microcracks propagate along grain-boundary ferrite even in microstructures predominantly consisting of acicular ferrite [13, 14].

Reduced values of impact strength in the temperature range of transition from ductile to brittle fracture are associated with ferrite grains having $\{001\}$ crystallographic cleavage planes located parallel to the fracture surface. The use of EBSD (electron back scatter diffraction) allows assessing the number and size of $\{001\}$ crystallographic clusters, which are considered as potential cleavage facets [15, 16], and relating the microstructure features to the fracture of samples tested for impact bending [17].

In this research, an attempt was made to establish the cause of different values of impact strength inside the weld when making a notch in the center and with an offset, using experimental data on the microstructure, impact strength, and fracture peculiarities of real welds from low-carbon low-alloy steel.

Material and Method

The object of research is a welded joint made by automatic multi-arc submerged arc welding. For welding, plates with dimensions of 2200×200×22 mm were used, selected from industrial sheet products from steel 07KhG2B, intended for the production of large-diameter pipes (LDP) of K60 strength class. Chemical composition of the weld is as follows, wt.%: C 0.07, Si 0.25, Mn 1.65, S 0.005, P 0.009, Al 0.04, Cr 0.20, Ni 0.01, Cu 0.015, Ti 0.020, N 0.010, Nb 0.050.

The plates were welded on a laboratory multi-arc welding rig in three stages (similar to the LDP welding technology):

(1) welding of the assembly joint (welding in a shielding gas environment);

(2) welding of the “inner” joint;

(3) welding of the “outer” joint.

Welding was carried out with increased heat input in a wide groove (the calculated cooling rate of the weld W8/5 was 3 °C/s). The volume of electrode metal required to fill a wide groove was provided by increasing the welding currents for three of the five electrodes of the multi-arc tandem.

Impact bending tests were carried out according to DIN EN ISO 14556 on a Zwick/Roell impact tester with an energy of 750 J. Ten nominally identical standard transverse samples from an outer weld with dimensions of 55×10×10 mm with a V-shaped notch were tested at a temperature of –40 °C. On five samples, the notch was applied along the axis of the outer weld; on other five samples, the notch was applied with a 3 mm offset so that it completely passed through the cast zone of the weld without touching the weld adjacent zones. The outer surface of the samples along the long side was located at a depth of 2 mm from the surface of the welded joint after grinding the bead.

The study of the macrostructure of the welded joint was carried out using a macro shooting system that included a Canon EOS 6D camera with a Canon MP-E 65 mm f/2.8 1–5 Macro lens. The break characteristics were analyzed using macrophotographs based on the technique used in [18]. The distance from the notch root to the upper boundary of the brittle fracture zone, which characterizes the initial propagation of a ductile main crack L, was measured. Break tightening Ψ was assessed as a percentage of the difference between the distance at the narrowest point of the break projection and the initial sample width to the initial width. Besides, the areas of shear lips, zones of uniform distribution of the main crack, rupture zones and zones of brittle fracture

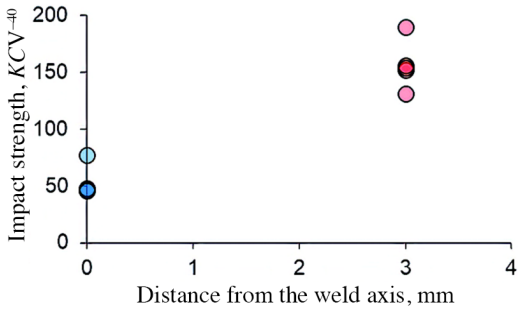

Fig. 1. Results of impact bending tests of samples of the outer weld. $T_{isp} = -40$ °C. Notch in the center of the weld is blue, notch with offset is red.

were determined. The share of the brittle component was determined as the percentage ratio of the brittle fracture projection area to the initial projection area of the sample under the notch.

The study of microfractographic features of breaks of the outer weld was carried out using a two-beam Crossbeam 1540 EsB (Carl Zeiss) device equipped with a Nordlyss S EBSD detector (Oxford Instruments) in the scanning electron microscope (SEM) mode. The accelerating voltage was 20 kV.

The microstructure was studied by optical microscopy and SEM in the EBSD mode. Shooting of EBSD cards was carried out with a step of 200–600 nm, 4×4 binning, a working length of 15 mm at an accelerating voltage of 20 kV and an aperture of 120 μm along a square raster. Crystallographic data were obtained and processed using the Aztec 3.1 and hkl Chanel 5 software (Oxford Instruments).

Metallographic thin sections for studying fracture processes were made from cross sections of broken samples perpendicular to breaks. To study the microstructure, samples were cut out from the outer weld in the transverse and longitudinal planes. Metallographic thin sections were prepared according to standard methods. To reveal the macro- and microstructure, a 2% alcoholic solution of HNO_3 was used. Metallographic thin sections for EBSD research after the standard procedure of sample preparation were subjected to polishing in a suspension of colloidal silicon with a grain size of 0.05 μm.

Experimental Results

Figure 1 presents the results of impact bending tests of transverse samples of the outer weld at a temperature of –40 °C.

The impact strength of samples with a notch in the center ranged from 46 to 77 J/cm^2, and the impact strength of samples with a notch with offset ranged from 131 to 190 J/cm^2.

Images of breaks and the results of quantitative macrofractographic analysis are shown in Fig. 2. The fracture of all samples began with the formation of a main ductile crack (blue zone) (see Fig. 2a). For samples with a notch in the center of the weld, the areas of initial propagation of a ductile crack, shear lips (highlighted in red) and rupture zones (highlighted in green) are smaller, and the brittle fracture area (highlighted in grey) is larger than that of samples with a notch with an offset. Fracture with low energy capacity is characterized by a large volume fraction of the brittle component (see Fig. 2b), a smaller distance from the notch to the upper edge of the brittle component L (see Fig. 2c) and a smaller tightening Ψ (Fig. 2d). With an increase in tightening Ψ, the volume fraction of the brittle component decreased (Fig. 2e). These differences indicate a lower degree of plastic deformation in samples with a notch in the weld center.

In a ductile crack near the notch root at the weld center, individual rare facets of a transcrystalline cleavage 100–550 μm long and 60–150 μm wide were observed (Fig. 3). In the fracture focus of such facets, spherical

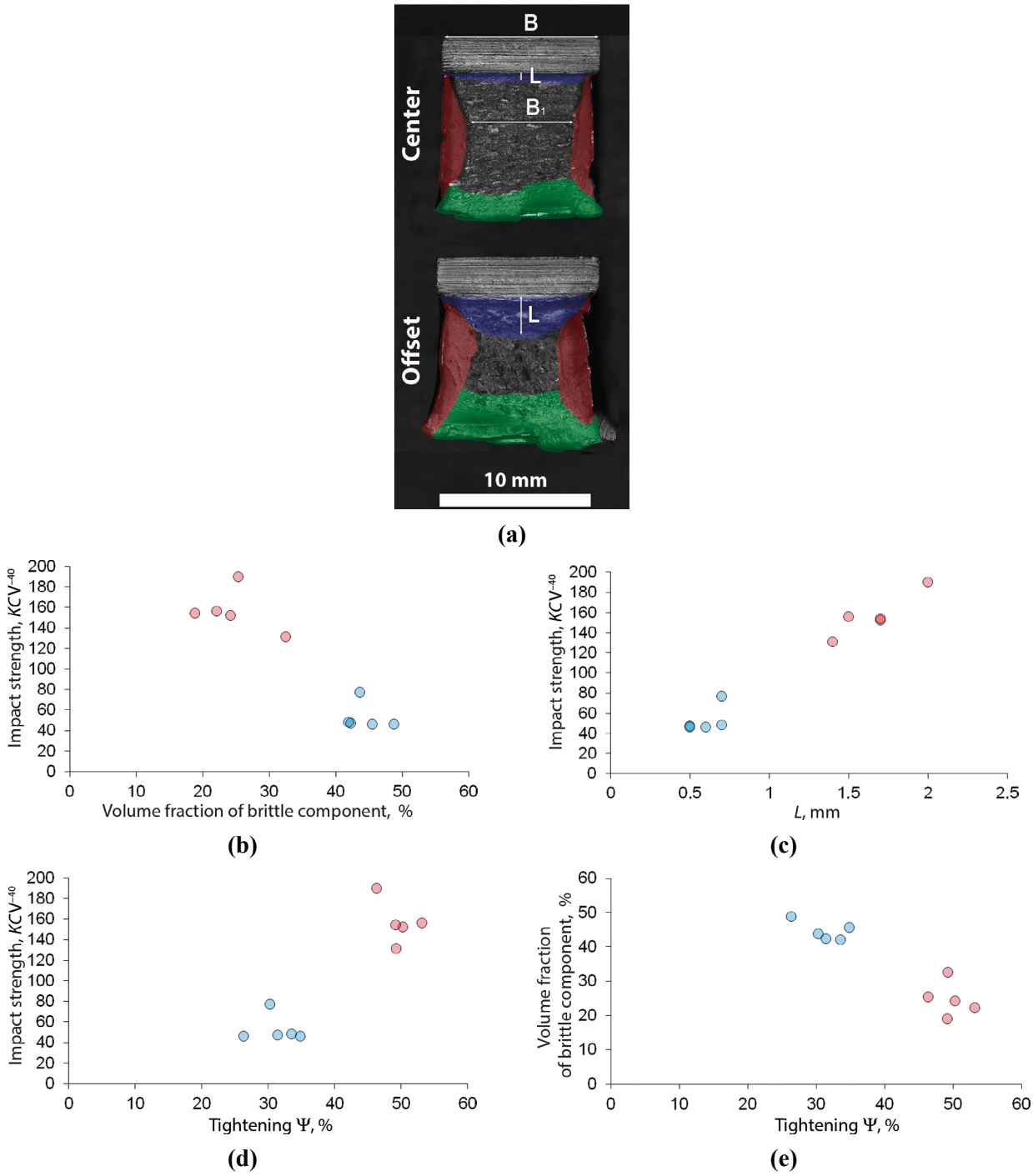

Fig. 2. Fractographic analysis of fracture surfaces of impact samples KCV^{-40}: (a) micrographs of breaks; (b) *KC*V — share of brittle component; (c) *KC*V — tightening; (d) *KC*V — distance from the notch to the brittle component; (e) share of brittle component — tightening. Zones: shear lips (red), rupture (green), uniform ductile crack propagation (blue), macrobrittle fracture (grey).

complex non-metallic Mn–Si–Al–Ca–S–Mg–Ti–O inclusions with a diameter of 3–5 μm that fell into the weld area from the flux were observed. On the surface of the same facets, Mn–Al–Si–Ti–S–O particles with sizes <0.6 μm were observed; however, these particles did not participate in the process of cleavage initiation.

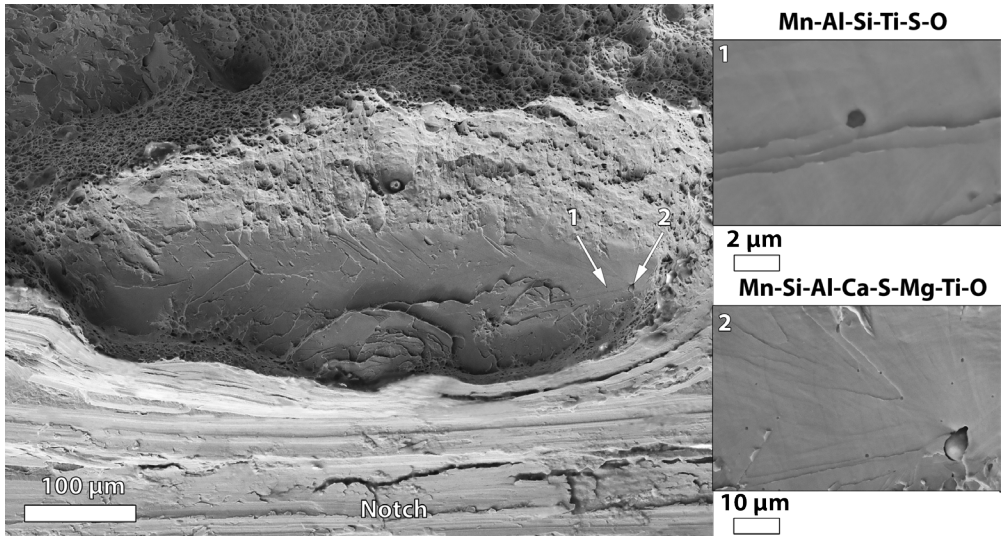

Fig. 3. Area of transcrystalline cleavage directly on the notch. Fracture of a sample with a notch in the center. SEM.

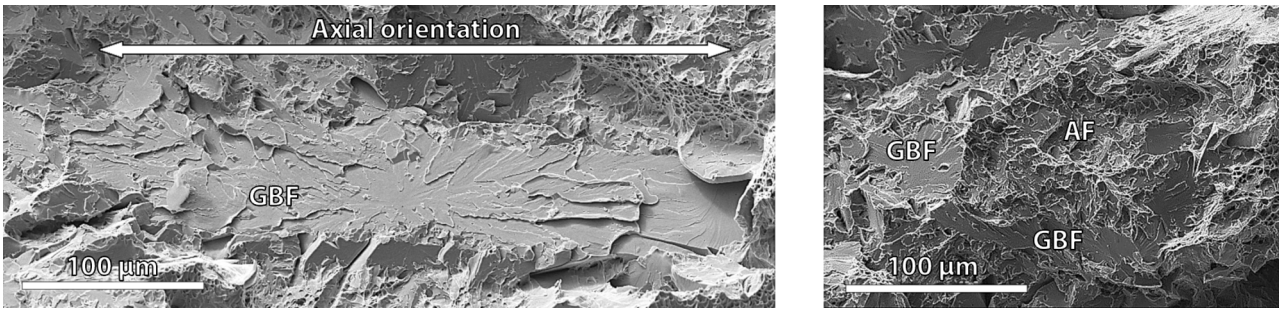

(a) **(b)**

Fig. 4. Areas of macroscopic brittle fracture, SEM: (a) notch in the center; (b) offset notch.

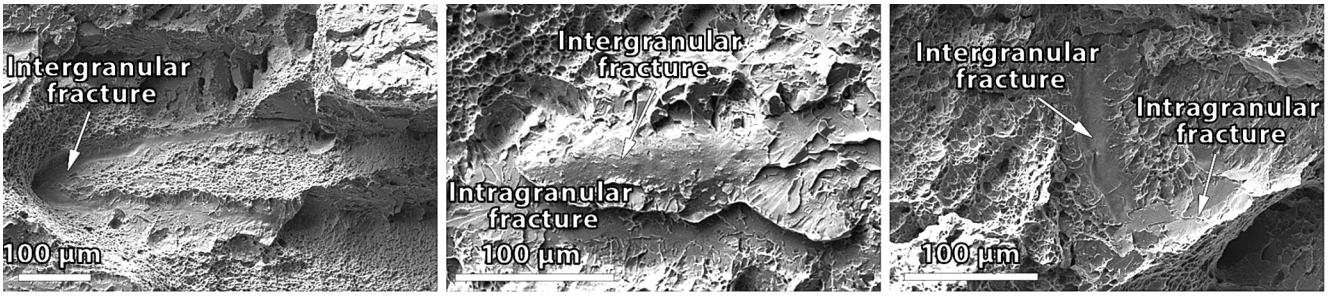

(a) **(b)** **(c)**

Fig. 5. Area of intergranular fracture, SEM: (a), (b) notch in the center; (c) offset notch.

Microscopic examination in the brittle fracture zone revealed facets of transcrystalline cleavage, as well as areas of quasi-cleavage and intergranular fracture (Figs. 4 and 5).

In the samples with a notch in the center, the cleavage occurred with the formation of a river pattern. Figure 4a shows a typical coarse transcrystalline facet elongated along the columnar grain axis. The shape, size and

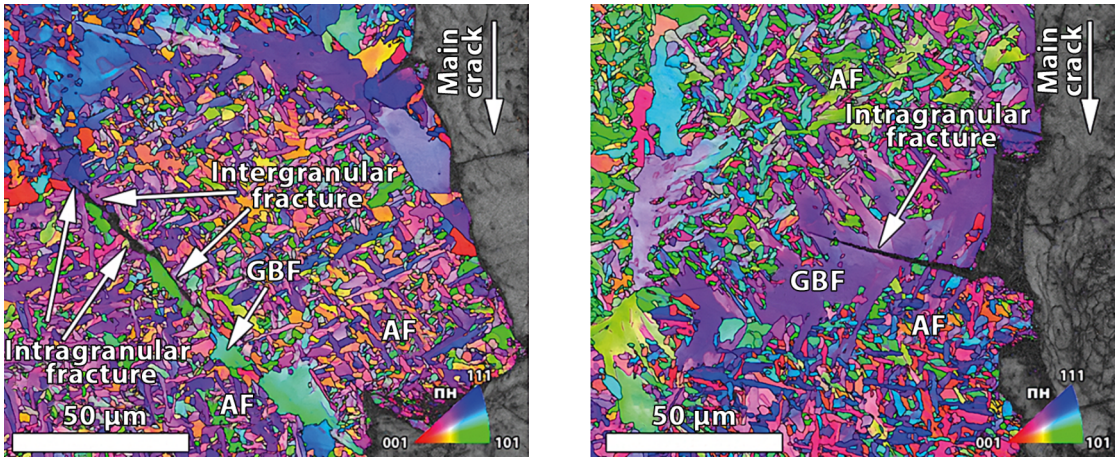

Fig. 6. Microcracks in the plastic zone. Cross section in the center. Notch in the center. Kikuchi image quality card BS + OTF. EBSD.

location of such facets indicate that the cleavage occurred mainly along the grain-boundary ferrite grains elongated along the boundaries of the former austenite.

In the samples with an offset notch, the brittle fracture was formed at angles of 50–60° to the columnar grains axis. The brittle fracture areas had a polygonal shape. In their central part, there were accumulations of small quasi-cleavage facets formed during the brittle fracture of acicular ferrite. In addition to their small size, they were distinguished by the absence of a river pattern and the presence of a large number of ridges. From the outside, the brittle polygonal areas are bordered by relatively large transcrystalline cleavage facets formed during the fracture of grain-boundary ferrite (see Fig. 4b).

In addition to the described cases, intergranular fracture was sometimes observed (see Fig. 5). In contrast to the cleavage and quasi-cleavage facets, the surface of the intergranular fracture zones was almost smooth with minor roughness.

Both in the breaks of samples with a notch in the center and samples with a notch with an offset, areas of intergranular fracture were observed. Such areas could border both on large facets of a transcrystalline cleavage (see Fig. 5a) and on clusters of small quasi-cleavage facets (see Fig. 5c). The spatial orientation of columnar crystallites predetermines a greater content and, accordingly, a greater contribution of intergranular fracture zones to the embrittlement of samples with a notch in the center (see Fig. 5b). Due to the inclination of columnar crystallites of lateral orientation with respect to the propagation front of the main crack, the formation of intergranular fracture areas was observed relatively rarely (Fig. 5c).

Figure 6 shows the orientation maps of the sections of the plastic zone of the sample fractured by impact bending.

Secondary microcracks in the plastic zone were observed in the area of grain boundaries of the former austenite: in acicular ferrite, in grain-boundary ferrite, and also at the boundary between these components of the microstructure. Figure 6a shows a microcrack, the trajectory of which has both segments of intergranular fracture between the zones of grain-boundary ferrite and acicular ferrite, and segments of intragranular transcrystalline fracture along acicular ferrite. Both tips of the residual microcrack are located in the areas of acicular ferrite. Another case is shown in Fig. 6b. Cleavage microcracks are formed in the areas of conjugation between acicular ferrite and grain-boundary ferrite. The main propagation trajectory of such cracks passes through the grains of grain-boundary ferrite. In the case of quasi-polygonal grain-boundary ferrite (QP GBF) with

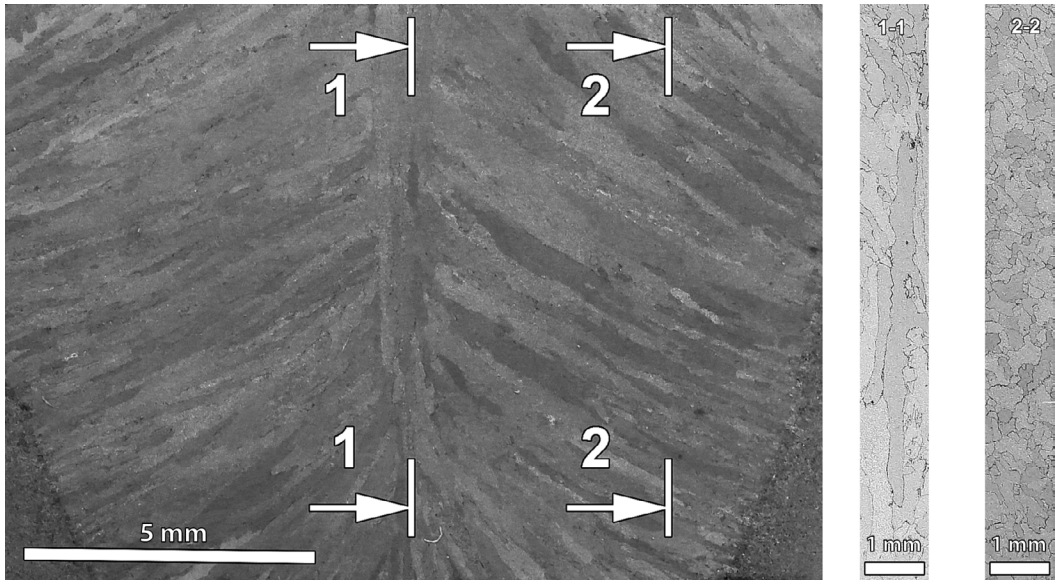

Fig. 7. Macrostructure of the longitudinal outer weld. Etching with 2% alcohol solution of HNO_3. OM: (a) cross section; (b) longitudinal section along the weld center (1–1); (c) longitudinal section with an offset of 3 mm from the weld axis (2–2).

Widmanstätten ferrite (WF) plates intertwined with adjacent areas of acicular ferrite, the crack crosses both the plates themselves and the acicular ferrite needles. Deceleration of residual microcracks in the cleavage occurs in the areas of acicular ferrite.

Figure 7 shows images of the macrostructure of the longitudinal outer weld in transverse and in two longitudinal sections (1–1) and (2–2).

A typical "tree-like" cast structure is observed in the cross section of the weld (see Fig. 7a). In the center are columnar grains of axial orientation elongated in the direction of the weld outer surface. Columnar grains of lateral orientation are located from the edges of the welded pipe billet towards the grains of axial orientation. The inclination angle between grains of axial and lateral orientation varies within 50–60°.

Figure 7b, c shows macrophotographs of the weld structure in longitudinal sections along the center and with an offset of 3 mm relative to the weld axis. In the longitudinal and transverse sections of the weld, columnar grains of axial orientation have a strongly elongated shape, Fig. 7a, b. The density of the boundaries of the former austenite in the longitudinal section along the center was 0.005 μm^{-1}, and in the longitudinal section with an offset — 0.011 μm^{-1}. The size of columnar grains of axial orientation in the longitudinal direction reached 6 mm. From the point of view of fracture in such a microstructure, the typical size in the longitudinal section is the width of the columnar grains, which was 238 μm ± 15 μm (see Table 1). In an offset longitudinal section, columnar grains of lateral orientation have a polygonal shape (see Fig. 7c). The typical size was 198 μm ± 7 μm.

Figure 8 shows EBSD maps and histograms of grain size distribution of structural components in the microstructure of the weld longitudinal sections.

The real microstructure consists of acicular and grain-boundary ferrites. The density of high-angle grain boundaries (>15°) of the real microstructure varied slightly in the longitudinal plane with distance from the center line of the weld. Since acicular and grain-boundary ferrites have a bcc lattice, their separation on orientation maps was carried out on the basis of a set of additional features: by the location of grains relative to the boundaries of columnar grains, by size, by shape, by crystalline lattice distortions, and local misorientations.

Table 1
Analysis of Microstructure Characteristics

Location	Former austenite		Real Structure				
			AF		GBF ferrite		
	Typical size (width), μm	Density of former austenite grain boundaries, μm^{-1}	Area weighted average equivalent diameter, μm	Maximum equivalent diameter, μm	Area weighted average equivalent diameter, μm	Maximum equivalent diameter, μm	Volume fraction, %
Center	238.4	0.005	10.2	46.8	51.7	137.7	14.0
Offset	198.2	0.011	9.4	58.8	33.7	79.5	16.7

Acicular ferrite was formed intragranularly within columnar grains on non-metallic inclusions (Fig. 9). Non-metallic inclusions were evenly distributed in the microstructure, regardless of the structure component. No dependence on their location with respect to columnar grains was observed. The areas of acicular ferrite show an increased concentration of local misorientations of 1–1.6° (green and yellow on the maps of average Kernel misorientations) (Fig. 9b). The weighted average equivalent grain diameter of acicular ferrite in longitudinal sections in the center and with an offset differed slightly: 10.2 and 9.4 μm, respectively. The maximum equivalent diameters were 46.8 and 58.8 μm. Acicular ferrite grains had an elongated shape with an average aspect ratio of 2.2 to 1. Intertwining randomly arranged needles provided an increased density of high-angle boundaries in the areas of acicular ferrite, regardless of the metallographic cross section: 0.94 μm^{-1} in the center and 0.90 μm^{-1} with an offset.

As a result of the $\gamma \rightarrow \alpha$ transformation, hypoeutectoid grain-boundary (primary) ferrite is generated along the boundaries of columnar grains. The grain-boundary ferrite zones are lighter on the Band slope maps (see Fig. 9a) and contain a reduced number of local misorientations of 1–1.6° on average Kernel misorientation maps (see Fig. 9b). The volume fraction of grain-boundary ferrite varies slightly depending on the cross section. In the longitudinal section, the volume fraction of grain-boundary ferrite is 14.0% in the weld center and 16.7% in the offset section. The area weighted average equivalent diameter of grains in longitudinal sections was 51.7 and 33.7 μm, and the maximum equivalent diameter was 137.7 and 79.5 μm, respectively.

Along the boundaries of the same columnar grain, equiaxed polygonal ferrite (GBF P1), elongated grains of polygonal ferrite (GBF P2), large grains of quasi-polygonal ferrite with a branched zigzag shape of boundaries (QP GBF) and grains of Widmanstätten ferrite (QP GBF + WF) could be released (see Fig. 9).

Grains of polygonal ferrite had both an equiaxed shape (GBF P1) with an aspect ratio of 1–1.5 to 1, and an elongated polygonal shape (GBF P2) with a ratio of the axes of the circumscribed ellipse reaching 6 to 1. The equivalent diameter of such grains did not exceed 60 μm. In contrast to the microstructure of the offset section in the longitudinal section along the weld center, the distribution of grain sizes contains a population of large grains of grain-boundary ferrite with an equivalent diameter of 60–135 μm. Such grain sizes were typical for quasi-polygonal grain-boundary ferrite (QP GBF) and quasi-polygonal grain-boundary ferrite with Widmanstätten needles (QP GBF + WF) (see Fig. 9). Both structural components are characterized by a branched

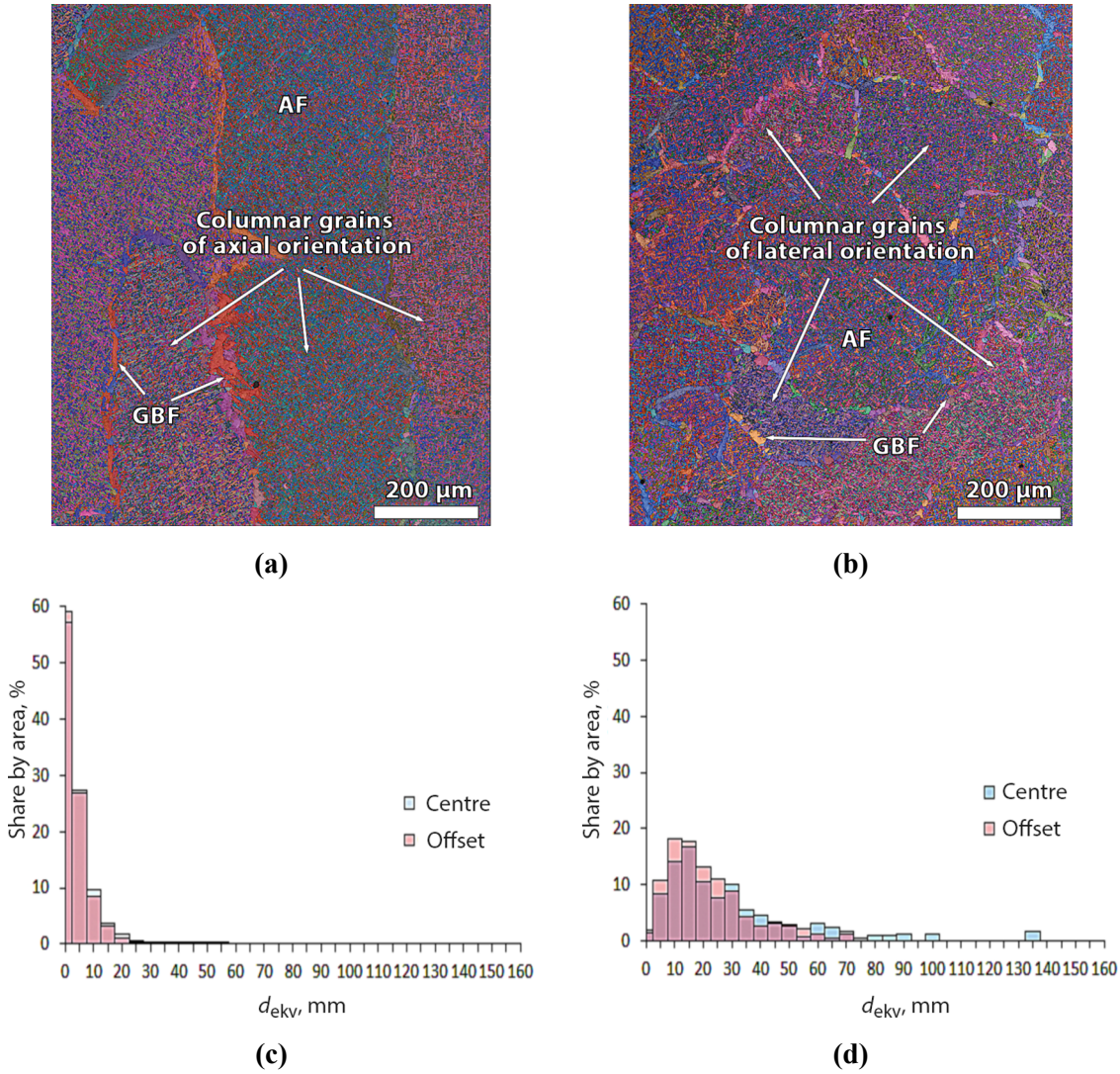

Fig. 8. Microstructure of the longitudinal outer weld. Step of 0.6 μm. Kikuchi Band Slope image quality map with overlay of Euler coordinates maps. Longitudinal section of the weld. EBSD: (a) section (1–1) in the center; (b) section (2–2) with an offset of 3 mm from the weld axis; (c) grain size distribution of acicular ferrite; (d) grain size distribution of grain-boundary ferrite.

morphology of grain boundaries, incomplete high-angle boundaries, and the presence of a substructure. The aspect ratio for such grains could reach 8 to 1. The formation of Widmanstätten ferrite was observed at high degrees of supercooling, as evidenced by the large proportion of the shear component. The substructure of such grains showed a lath-polygonal character.

Crystallization of a weld with a predominant crystallographic direction [100] implies the influence of microtexture on fracture processes. The brittle fracture of α-iron occurs as a transcrystalline cleavage along the {001} planes. This gives grounds to use the concept of local "potential cleavage facets" or {001} crystallographic clusters [15] to analyze the tendency to transcrystalline cleavage of such a microstructure. The condition for crack propagation from one grain to another is a small misorientation of the cleavage planes in neighboring grains. Thus, in this research, {001} crystallographic clusters were taken to be areas of the microstructure, the cleavage planes of which were misoriented within 20° with respect to the plane parallel to the notch plane (longitudinal plane) [16]. Taking into account the fact that the largest facets of a transcrystalline cleavage lead to less

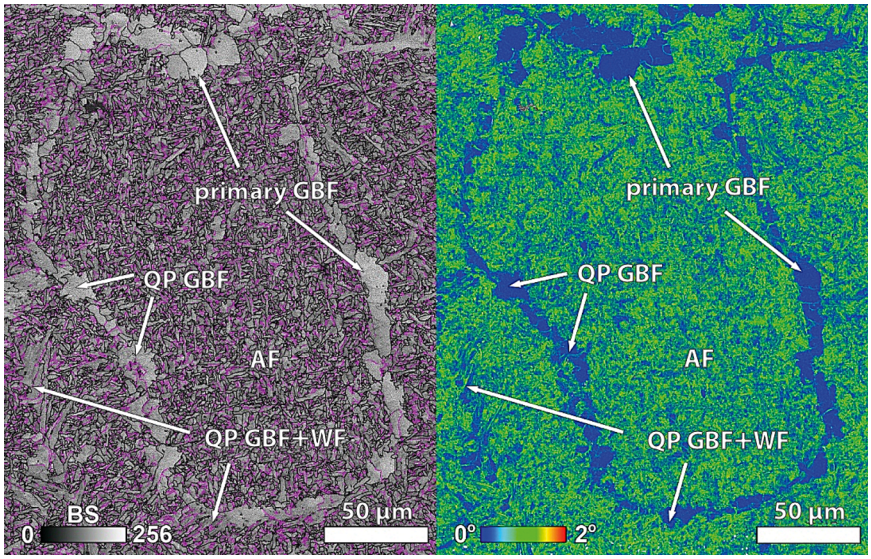

Fig. 9. Various morphologies of grain boundary ferrite, outlining one grain of former austenite: (a) Kikuchi Band Slope image quality map; (b) map of Kernel average misorientations. Longitudinal section with an offset relative to the weld axis. EBSD.

energy-intensive fractures, the assessment of the distribution of the area-reduced average equivalent diameter of crystallographic clusters with an emphasis on the "tail" of large values seems appropriate.

Figure 10 shows orientation maps of {001} crystallographic clusters and their size distributions depending on the microstructure component for two longitudinal sections.

The volume fraction of {001} clusters in the cross section along the weld center was 13.7%, in the cross section with an offset — 14.8%, and in the base metal — 13%. At that, potential places of cleavage nucleation were observed both in acicular ferrite and in grain-boundary ferrite. The content of {001} crystallographic clusters correlated with the content of structural components in the microstructure. In the section along the weld center, 86% of the acicular ferrite corresponded to 11.4% of the potential cleavage facets; in the section with an offset, 83.3% corresponded to 12.5%; in the central section, 14% of acicular ferrite corresponded to 2.3% of {001} crystallographic clusters; in the section with an offset, 16.7% corresponded to 2.3%.

The size distribution of {001} clusters for acicular ferrite and grain-boundary ferrite is shown in Fig. 10d, e. The area weighted average equivalent diameter of {001} crystallographic clusters in acicular ferrite was 11.6 μm in the section along the weld center and 12.6 μm in the section with an offset. The maximum equivalent diameter of acicular ferrite clusters was 55 μm. The area weighted average equivalent diameter of {001} crystallographic clusters in the zones of grain-boundary ferrite was significantly larger than in the zones of acicular ferrite and amounted to 56 and 34.5 μm in the longitudinal plane along the center and with an offset. In the section along the center in the size distribution of {001} clusters for grain-boundary ferrite, clusters of equivalent diameters of 155 μm were observed. Such clusters corresponded to areas of the microstructure with large (80–135 μm) grains of quasi-polygonal grain-boundary ferrite and quasi-polygonal grain-boundary ferrite with Widmanstätten plates. In the microstructure of the section with an offset relative to the weld axis, the maximum equivalent diameter of the {001} crystallographic clusters was 90 μm, which correlated with the size of the largest grains in the section (Table 1).

The content of {001} crystallographic clusters in columnar grains varies depending on their crystallographic orientation (see Fig. 10a–c). An "alternation" of columnar grains with a higher and lower content of potential

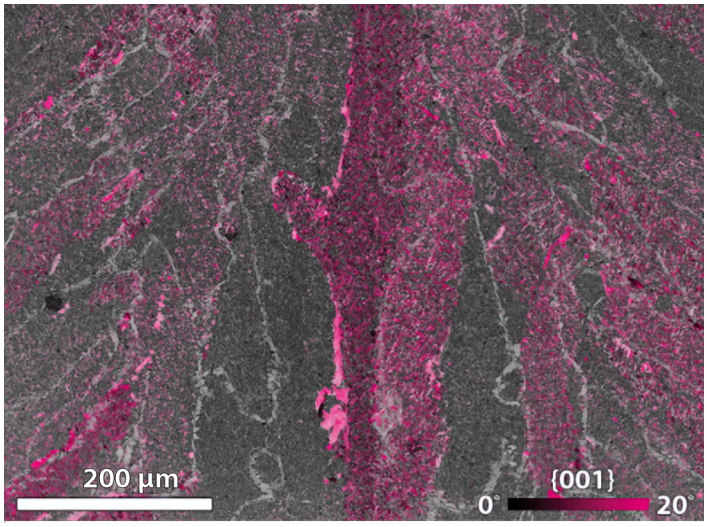

(a)

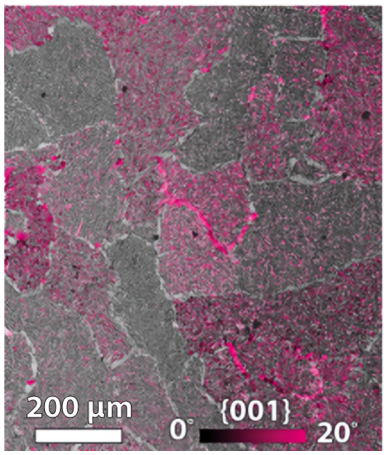

(b)

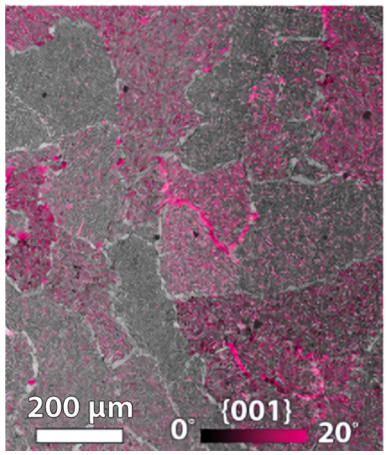

(c)

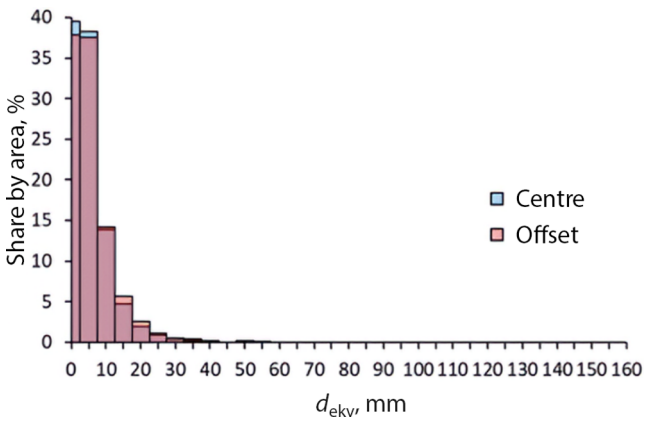

(d)

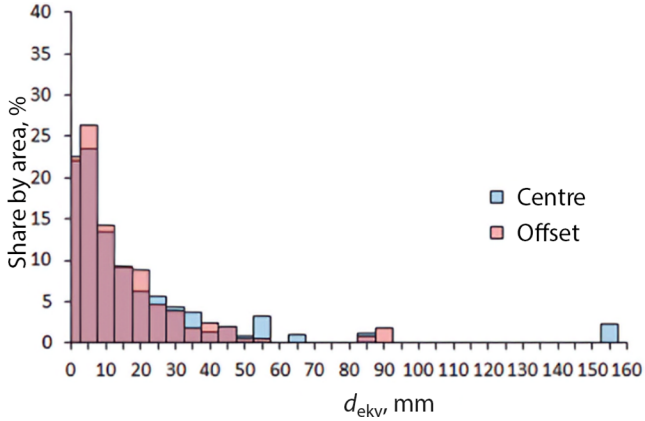

(e)

Fig. 10. Clusters of cleavage planes {001}: (a) cross section; (b) longitudinal section in the center; (c) longitudinal section with an offset of 3 mm from the weld axis; (d) size distribution of {001} clusters of acicular ferrite in the longitudinal section; (e) size distribution of {001} clusters of grain boundary ferrite in the longitudinal section.

cleavage facets was observed. In adjacent grains of former austenite, the content of potential cleavage facets varied in the range of 0.5–23.5%.

Discussion of the Results

Shown in Fig. 7, the microstructure is the result of several successive transformations during crystallization and cooling of the liquid pool of the weld. It is shown that such a structure has a distinct microtexture closely related to the predominant crystallographic direction of primary crystallization [100] (see Fig. 10). Primary crystallization occurs with the inheritance of the orientation of the solid support [1–3]. For columnar grains of lateral spatial orientation, such a support is the edges of the pipe billet heated to melting temperatures, for columnar grains of axial spatial orientation — the inner weld metal. Reheating leads to an almost random orientation of the support grains.

The fact that the polymorphic transformation occurs from δ-ferrite to γ-austenite is indicated by the uniform arrangement of non-metallic inclusions through the entire volume of the weld [12]. During the $\gamma \rightarrow \alpha$ transformation along the grain boundaries of the former austenite, grain-boundary ferrite of various morphologies is formed, and inside the grains of the former austenite, many grains of acicular ferrite appear on non-metallic inclusions.

Grain-boundary ferrite grains show an orientation relationship with the former austenite grains in which they grow. Grains of acicular ferrite show an orientation relationship both with the grains of the former austenite and with non-metallic inclusions on which they originated [19, 20].

The non-random nature of the transformation leads to the fact that in adjacent grains of the former austenite rotated relative to each other, the formation of a limited number of grain orientations of the real microstructure and, accordingly, the presence of unfavorably oriented $\{001\}$ cleavage planes with respect to the notch plane are observed (Fig. 10). The "alternation" of the microstructure sections with favorably and unfavorably oriented cleavage planes leads to difficulties in the propagation of transcrystalline fracture. The density of the grain boundaries of the former austenite reduced by half and the larger typical size in the longitudinal weld sections (for grains of axial orientation — width, for grains of lateral orientation — diameter) (see Table 1), lead to the fact that the transition of the main crack from a former austenite grain with a high content of $\{001\}$ cleavage planes to a grain with a lower content occurs less frequently in the center and more often with an offset. Apparently, these effects also affect the plastic properties of the metal [21, 22] (see Fig. 2): the degree of plastic deformation during the fracture of samples with a notch in the center of the weld is lower.

The size and content of acicular ferrite weakly depend on the spatial orientation of the former austenite grains (see Table 1). First of all, the microstructure dispersity of acicular ferrite is determined by the number of intragranular nucleation centers and the cooling rate during the $\gamma \rightarrow \alpha$ transformation [8, 9].

The formation of a continuous grid of grain-boundary ferrite by itself reduces the strength of the weld [13, 14]. In the longitudinal section with an offset of 3 mm, a somewhat higher (by 2.7%) content of grain-boundary ferrite is observed. In its turn, the anisotropic shape of the columnar grains leads to the formation of larger grains of grain-boundary ferrite along the elongated sides of the columnar grains. The weighted average and maximum equivalent diameters of grain-boundary ferrite grains are significantly larger in the longitudinal section along the center (51.7 μm versus 33.7 μm and 137.7 μm versus 79.5 μm). This, apparently, is due to the larger surface of the former austenite available for the growth of grain-boundary ferrite at the moment of the $\gamma \rightarrow \alpha$ transformation. The largest grains of grain-boundary ferrite belong to quasi-polygonal ferrite and quasi-polygonal ferrite with Widmanstätten plates [6, 23] (see Fig. 9). In contrast to acicular ferrite, in which cleavage cracks are retarded due to the formation of a fine-grained intertwining microstructure, in such grains the free path of cleavage microcracks is maximum (Fig. 3, Fig. 6b).

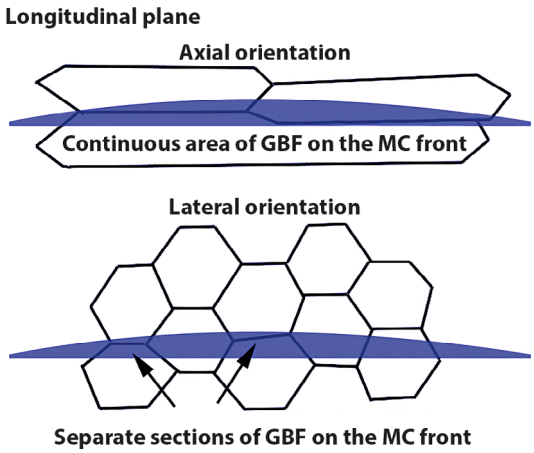

Fig. 11. Schematic representation of the fracture process of columnar grains of axial and lateral spatial orientations in the longitudinal plane. MC is the main crack.

The combination of large grains of grain-boundary ferrite and non-metallic inclusions of 3–5 μm in the case of falling on the front of the main crack leads to a cleavage at an early stage of fracture in the samples in the weld center (see Fig. 3). In addition, the formation of grain-boundary ferrite of a different nature along the boundaries of the same grains of the former austenite in itself indicates the unequal course of the $\gamma \rightarrow \alpha$ transformation under conditions of an equivalent temperature field. It seems that under such conditions the course of transformation is primarily determined by the inhomogeneity of the local chemical composition along the boundaries of columnar grains.

According to the above, the location of a continuous chain of grains of grain-boundary ferrite along the boundaries of columnar grains of axial orientation along the notch line parallel to the front of the main crack increases the tendency to transcrystalline cleavage (Fig. 11).

In contrast to this, the location of only separate sections of grain-boundary ferrite parallel to the notch in the longitudinal section of the weld with an offset reduces the tendency to brittle fracture.

Thus, under conditions of reduced plasticity, the main contribution to the decrease in impact strength in the center of the cast zone of the outer weld is made by a combination of large grains of grain-boundary ferrite with an unfavorable orientation of cleavage planes and non-metallic inclusions.

An additional contribution to the decrease in the values of impact strength in the center of the outer weld was made by intergranular fracture (see Figs. 5 and 6). Areas of such fracture were encountered more often than in the section with an offset due to the coincidence of the propagation trajectory of the main crack with the surface of the boundary between acicular ferrite and grain-boundary ferrite in columnar grains of axial orientation. The authors assume that this type of fracture is similar to the case typical for the formation of splittings [24, 25]. The formation of intergranular fracture is due to the inhomogeneity of plastic deformation gradients between microstructure components of different sizes and defectiveness degrees.

CONCLUSIONS

1. It has been established that the size and spatial orientation of the columnar grains of the former austenite, the size, shape and location of the grain-boundary ferrite grains, their combination with non-metallic inclusions, as well as the size of $\{001\}$ crystallographic clusters parallel to the fracture plane, affect the impact strength of the weld.

2. The main reason for the reduced values of impact strength of samples with a notch in the weld center is the existence of a fraction of large grains of grain-boundary ferrite with an equivalent diameter of 80–140 μm elongated along the notch-parallel boundaries of the columnar grains of the former austenite of axial orientation. The combination of such grains and non-metallic inclusions 3–5 μm in size facilitates the formation of focal facets of a transcrystalline cleavage near the notch and increases the share of the brittle component in breaks.

3. With the axial orientation of the columnar grains of the former austenite, the main crack front passes along a continuous chain of grain-boundary ferrite grains, lined up along the boundaries of the columnar grains parallel to the notch, which increases the tendency to transcrystalline cleavage. At the same time, with the lateral orientation of the columnar grains of the former austenite, the main crack front crosses only individual grains of grain-boundary ferrite.

4. The share of {001} crystallographic clusters in the break plane is 13–14% and it slightly differs in the section along the weld center, in the section with an offset, and in the section of the pipe wall. However, their size distribution differs significantly. The largest {001} clusters 160 μm in size were observed only in the section along the weld center, in areas of the microstructure with large grains of grain-boundary ferrite. This imposes an embrittling effect on the weld metal.

5. In adjacent grains of former austenite, the share of potential cleavage facets varied within 0.5–23.5%. In the case of fracture along grains of lateral orientation, a more frequent alternation of microstructure sections with favorably and unfavorably oriented cleavage planes leads to difficulties in the propagation of transcrystalline fracture.

6. Separate areas of intergranular fracture observed at the boundaries between acicular ferrite and grain-boundary ferrite should be considered as an additional embrittling factor. A greater content of such areas was observed during the fracture of samples with a notch in the center.

Part of the research was carried out within the framework of the State Task 075-01176-23-00.

REFERENCES

1. K. Easterling, *Introduction to the Physical Metallurgy of Welding. Second Edition*, Butterworth-Heinemann, Oxford (1992).
2. S. Kou, *Welding Metallurgy. 3rd Ed.*, John Wiley & Sons, Hoboken (2020).
3. J. C. Lippold, *Welding Metallurgy and Weldability*, John Wiley & Sons, Hoboken (2014).
4. S. V. Zharkov, P. P. Stepanov, A. V. Chastukhin, et al., "Patterns (research) of effect of microstructure on impact strength of welded joints of large diameter pipes," *Metallurg*, No. 9, 13–22 (2022).
5. J. C. F. Jorge, L. F. G. de Souza, M. C. Mendes, et al., "Microstructure characterization and its relationship with impact toughness of C-Mn and high strength low alloy steel weld metals: A review," *J. Mater. Res. Technol.*, **10**, 471–501 (2021).
6. O. A. Bagmet, P. P. Stepanov, S. V. Zharkov, et al., "Features of formation of the structure of a welded joint made by automatic submerged arc welding," *Probl. Chern. Metallurg. Materialoved.*, No. 2, 52–65 (2022).
7. M. Diaz-Fuentes, A. Iza-Mendia, and I. Gutierrez, "Analysis of different acicular ferrite microstructures in low-carbon steels by electron backscattered diffraction. Study of their toughness behavior," *Metall. Mater. Trans. A*, **34**, 2505–2516 (2003).
8. L. Cho, A. Tselikova, K. Holtgrewe, et al., "Critical assessment 42: acicular ferrite formation and its influence on weld metal and heat-affected zone properties of steels," *Mater. Sci. Technol.*, **38**, No. 17, 1425–1433 (2022).
9. Y. Shao, C. Liu, Z. Yan, et al., "Formation mechanism and control methods of acicular ferrite in HSLA steels: A review," *J. Mater. Sci. Technol.*, **34**, No. 5, 737–744 (2018).
10. D. Loder, S. K. Michelic, and C. Bernhard, "Acicular ferrite formation and its influencing factors: A review," *J. Mater. Sci. Res.*, **6**, No. 1, 24–43 (2016).
11. F. J. Barbaro, P. Krauklis, and K. E. Easterling, "Formation of acicular ferrite at oxide particles in steels," *Mater. Sci. Technol.*, **5**, No. 11, 1057–1068 (1989).

12. H. K. D. H. Bhadeshia and L. E. Svensson, "Modelling the evolution of microstructure in steel weld metal," in: H. Cerjak and K. E. Easterling (eds.), *Mathematical Modelling of Welding Phenomena*, Institute of Materials, London (1993).
13. J. S. Seo, H. J. Kim, and H. S. Ryoo, "Effect of grain boundary ferrite on susceptibility to cold cracking in high-strength weld metal," *Met. Mater. Int.*, **14**, No. 4, 515–522 (2008).
14. Z. Shi, T. Pan, Y. Li, et al., "Mechanism of BN-promoting acicular ferrite nucleation to improve heat- affected zone toughness of VN–Ti microalloyed offshore steel," *Materials*, **15**, No. 4, 1420 (2022).
15. F. Tankoua, J. Crépin, P. Thibaux, et al., "Quantification and microstructural origin of the anisotropic nature of the sensitivity to brittle cleavage fracture propagation for hot-rolled pipeline steels," *Int. J. Fracture*, **212**, 143–166 (2018).
16. A. Gervasyev, I. Pyshmintsev, R. Petrov, et al., "Splitting susceptibility in modern X80 pipeline steels," *Mater. Sci. Eng. A*, **772**, No. 2, 138746 (2020).
17. M. M. Kantor, K. G. Vorkachev, and K. A. Solntsev, "Nature of the scatter in the impact toughness of low-carbon low-alloy steel during fracture under ductile-brittle transition conditions," *Neorgan. Mater.*, **56**, No. 11, 1271–1276 (2020).
18. M. M. Kantor, K. G. Vorkachev, V. A. Bozhenov, and K. A. Solntsev, "The role of splitting phenomenon under fracture of low-carbon microalloyed X80 pipeline steels during multiple Charpy impact tests," *Appl. Mech.*, **3**, No. 3, 740–756 (2022).
19. A. O. Kluken, Ø. Grong, and J. Hjelen, "The origin of transformation textures in steel weld metals containing acicular ferrite," *Metall. Trans. A*, **22**, 657–663 (1991).
20. H. Nako, H. Hatano, Y. Okazaki, et al., "Crystal orientation relationships between acicular ferrite, oxide, and the austenite matrix," *ISIJ Int.*, **54**, No. 7, 1690–1696 (2014).
21. M. Shi, M. Di, J. Zhang, et al., "Effect of initial microstructure on the toughness of coarse-grained heat-affected zone in a micro-alloyed steel," *Materials*, **14**, No. 16, 4760 (2021).
22. X. Li, G. Lu, Q. Wang, et al., "The effects of prior austenite grain refinement on strength and toughness of high-strength low-alloy steel," *Metals*, **12**, No. 1, 28 (2021).
23. J. Yin, M. Hillert, and A. Borgenstam, "Morphology of proeutectoid ferrite," *Metall. Mater. Trans. A*, **48**, 1425–1443 (2017).
24. H. Herø, J. Evensen, and J. D. Embury, "The occurrence of delamination in a control rolled HSLA steel," *Can. Metall. Quart.*, **14**, No. 2, 117–122 (1975).
25. H. L. Haskel, E. Pauletti, J. D. P. Martins, and A. L. M. de Carvalho, "Microstructure and microtexture assessment of delamination phenomena in Charpy impact tested specimens," *Mater. Res.*, **17**, No. 5, 1238–1250 (2014).